Locating Magnetic Reconnection at Earth's Dayside Magnetopause in Global Magnetospheric Simulations

Colin M. Komar, Department of Physics, *West Virginia University*

1 Statement of the Problem

The transfer of energy and mass from the solar wind into the magnetosphere is governed by magnetic reconnection, which occurs when magnetic fields with oppositely directed components merge and nullify. This process is of critical importance to space weather, as it controls magnetospheric convection (*Dungey*, 1961) and energy release during geomagnetic storms and substorms (*Angelopoulos et al.*, 2008). Conditions in the solar wind determine the efficiency and location of reconnection at the dayside magnetopause, which in turn determines the efficiency of solar wind-magnetospheric coupling. In particular, as pointed out by *Dungey* (1961, 1963), when the interplanetary magnetic field (IMF) is southward as sketched in Fig. 1, reconnection happens at the red box near the subsolar point, which allows the magnetic field to be stretched into the magnetotail and the transfer of energy from the solar wind is efficient. When the IMF points northward, reconnection happens near the polar cusps, and the energy transfer from the solar wind is inefficient.

The examples of northward and southward IMF are special cases which are well understood because of the high degree of symmetry. However, despite the importance of this process, much less is known about where reconnection occurs for arbitrary IMF clock angles $\theta_{\rm IMF}$. It is not presently possible to *quantitatively* predict the efficiency or even the location of magnetic reconnection at Earth's dayside magnetopause for arbitrary IMF clock angles $\theta_{\rm IMF}$. Understanding where reconnection occurs for different clock angles is also important to inform observational studies of magnetopause reconnection where they should go into data collection mode. Therefore, understanding magnetopause reconnection for arbitrary clock angle could directly benefit NASA's upcoming Magnetospheric Multi-Scale (MMS) mission, a satellite mission specifically designed to study properties of magnetic reconnection at small length scales at Earth's magnetosphere.

Predicting where reconnection occurs at the dayside magnetopause is very difficult because it is a fully three-dimensional problem. For the southward IMF case in Fig. 1, the location of reconnection is relatively easy to find; it is the point in the red box on the left where open solar wind magnetic field lines meet closed terrestrial field lines, which also lies at the boundary with half-open newly reconnected field lines that map to the Earth in only one direction. This point is part of a line called the "magnetic separator," so-called because it separates regions of different magnetic topology (*Cowley*, 1973; *Siscoe*, 1987; *Lau and Finn*, 1990; *Siscoe et al.*, 2001). When the IMF is not due northward or southward, the magnetic field structure of the magnetosphere becomes very complicated. However, there is still a magnetic field line that separates different topologies of magnetic field lines, and this separator continues to be the location where reconnection is likely to occur. Thus, identifying the dayside reconnection site requires locating the separator.

The present project is to locate separators on the dayside magnetopause in global magnetospheric simulations using a technique developed by the applicant (*Komar et al.*, submitted to J. Geophys. Res.). The

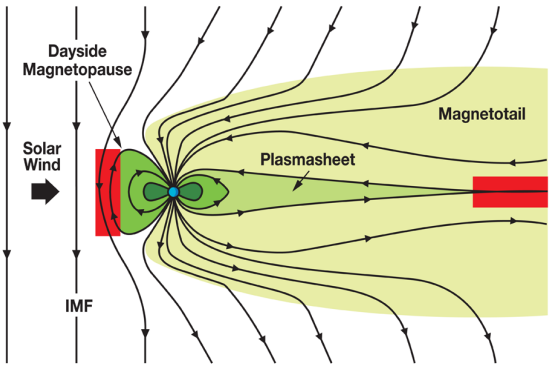

Figure 1: Schematic sketch of Earth's magnetosphere. Image courtesy of MMS (NASA/SWRI).

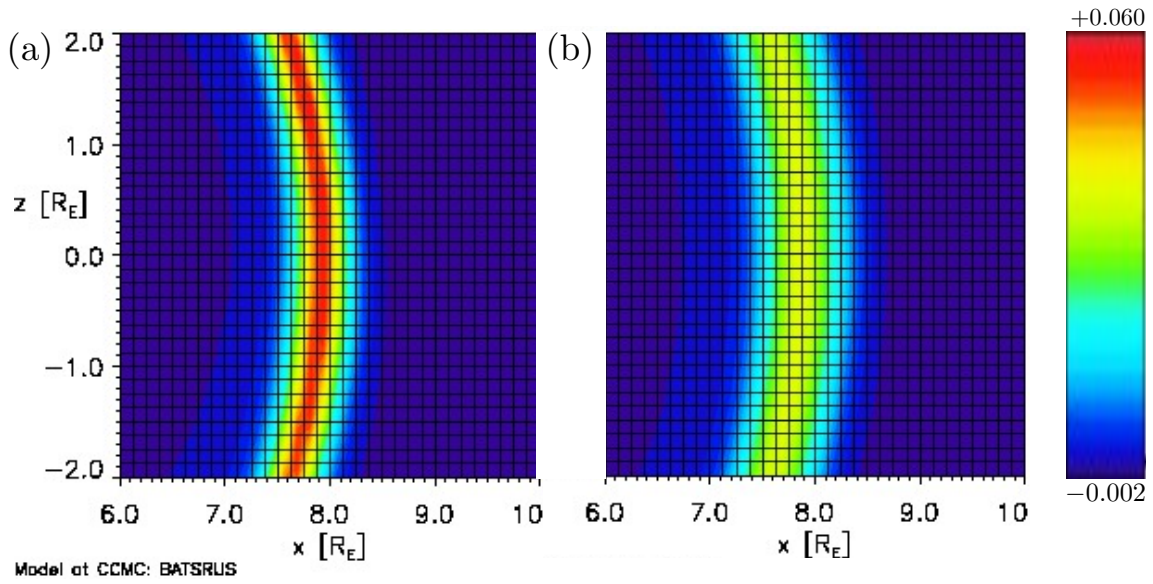

Figure 2: Magnetopause current density J_y $\left(\mu\mathrm{A/m}^2\right)$ near the subsolar point in simulations (a) without an explicit resistivity and (b) with an explicit resistivity $\eta/\mu_0 = 6.0$ m^2/s. The current layer broadens in (b), demonstrating the explicit resistivity dominates numerical effects. Solid (black) lines indicate the simulation grid (0.125 $\mathrm{R_E}$).

technique exploits the property of magnetic separators that they begin and end on magnetic nulls, where the magnetic field strength goes to 0. Starting at a magnetic null, the point where the separator pierces a small sphere centered at the null is located using resources from CCMC. This point is used as the center for another sphere, and the technique is iterated until it reaches the other null. This technique is verified against exact solutions for separators in an analytic magnetic field model. The new technique is more efficient than existing methods and is highly accurate, and works for arbitrary clock angle unlike some existing methods. Separators are found in global resistive magnetohydrodynamic (MHD) simulations with clock angles ranging from 0° to 180° run at CCMC. Trends in magnetic null locations and the structure of magnetic separators as a function of clock angle are presented and compared with those from the analytic field model. There are many qualitative similarities between the two models, but quantitative differences are also noted. Dependence on solar wind density is briefly investigated.

2 Description of CCMC Models and Tools Used

2.1 Magnetospheric Simulation Study

Investigating magnetic reconnection at Earth's dayside magnetopause requires a model with a self-consistently generated magnetosphere and dissipative effects that allow magnetic reconnection. We use the Block-Adaptive-Tree-Solarwind-Roe-Upwind-Scheme (BATS-R-US) (*Powell et al.*, 1999; *Gombosi et al.*, 2000; *De Zeeuw et al.*, 2000), using CCMC's Runs-On-Request service. BATS-R-US solves the MHD equations on a three-dimensional rectangular irregular grid. The simulation domain is $-255 < x < 33, -48 < y < 48, -48 < z < 48$, where distances are measured in $\mathrm{R_E}$ and the coordinate system is Geocentric Solar Ecliptic (GSE); in GSE coordinates, x is sunward, y is duskward, and z is northward.

The simulations are run using BATS-R-US version 8.01 and do not use the Rice Convection Model (RCM). The simulations are evolved for two hours (02:00:00) of magnetospheric time. We look at the 02:00:00 mark of simulation data because the system has achieved a quasi-steady state; the magnetopause current layer along the x-axis is approximately stationary. The standard high-resolution grid for CCMC simulations has $1,958,688$ grid cells with a coarse resolution of 8 $\mathrm{R_E}$ in the far magnetotail, and a fine resolution of 0.25 $\mathrm{R_E}$ near the magnetopause. The present study employs a higher resolution grid of 0.125 $\mathrm{R_E}$ packed in the region

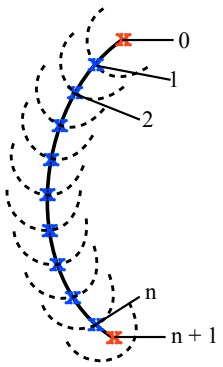

Figure 3: Schematic diagram of the separator tracing algorithm.

$-6 < x < 10, -10 < y < 10, -5 < z < 5$ R_E with 3,736,800 total grid cells.

Our initial simulations use fixed solar wind inflow conditions and do not employ a dipole tilt for simplicity. The solar wind has temperature $T = 232,100$ K, IMF strength 20 nT, number density $n = 20$ cm^{-3}, and a solar wind velocity of $\mathbf{v} = -400$ km/s $\hat{\mathbf{x}}$. We perform distinct simulations with IMF clock angle $\theta_{\text{IMF}} = 0°$ (parallel), 30°, 60°, 90°, 120°, 150°, 165°, and 180° (anti-parallel). The IMF does not have a B_x component. Constant Pederson and Hall conductances of 5 mho are used. The solar radio flux F10.7 index is set at a value of 150. We employ a uniform explicit resistivity $\eta/\mu_0 = 6.0 \times 10^{10}$ m^2/s in all of our simulations. It is known that the magnetosphere is not collisional, but including an explicit resistivity allows for reproducible results that are independent of the numerics. To ensure this resistivity controls the dissipation instead of the numerics, we show J_y in the $y = 0$ plane at the dayside magnetopause in Fig. 2 for (a) no explicit resistivity and (b) with the explicit resistivity. The current layer broadens, suggesting the explicit resistivity is controlling the dissipation, as desired.

We perform additional simulations to address the separators' dependence on a variety of simulation parameters. In a simulation with $\theta_{\text{IMF}} = 30°$, we change the solar wind number density for $n = 20$ cm^{-3} to 5 cm^{-3} as an initial parametrization test of separator dependence on solar wind conditions. To confirm sufficient resolution in the simulations to accurately determine magnetic separators, we perform a series of simulations where the high resolution domain is increased for certain IMF clock angles; in some cases, the aforementioned high resolution domain did not fully contain the separators. The additional simulations have IMF with clock angles $\theta_{\text{IMF}} = 60°$, 150°, and 165°. The same solar wind conditions are used, except the 0.125 R_E resolution region with $\theta_{\text{IMF}} = 60°$ spans $-6 < x < 10, -10 < y < 10, -12 < z < 12$ R_E and $-6 < x < 10, -15 < y < 15, -10 < z < 10$ R_E for the two southward IMF simulations. We find that our initial simulation parameters were sufficient to obtain accurate null locations and separators; see *Komar et al.* (submitted to J. Geophys. Res.) for details.

2.2 Visualization and Processing of Simulation Results

We make use of several different tools and services available at CCMC. Figure 2 was generated using the On-Line Visualization resources at the CCMC. A large portion of the analysis presented here was made possible via the Kameleon and Space Weather Explorer software packages provided by the CCMC. Kameleon was used to determine field line topology by performing bi-directional traces of magnetic field lines from arbitrary seed points and to interpolate simulation data into regularly sampled grids for further data processing. Additionally, Kameleon was used to generate magnetic field lines in Fig. 8 for comparison with the magnetic separators. Space Weather Explorer was used to visualize magnetic field lines to check our characterization of magnetic topologies, magnetic nulls and separators.

3 Theory - A Technique for Finding Separators

The separator tracing algorithm developed by the applicant exploits the fact that magnetic nulls are the endpoints of magnetic separators. A schematic diagram of the tracing process is shown in Fig. 3. The two

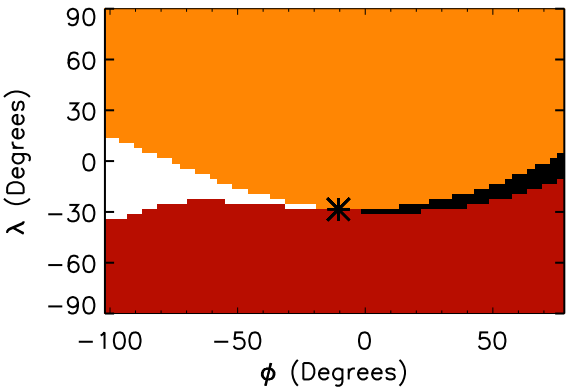

Figure 4: Sample topology map for $\theta_{\rm IMF} = 30^\circ$ for a hemisphere centered at $\mathbf{r} = (3.16, 1.87, 8.01)$ R_E, with radius of 1 R_E. Colors denote magnetic topology: red are closed terrestrial fields, orange are open solar wind fields, black and white are half-closed fields that terminate at the south and north poles of Earth, respectively. The black asterisk marks the approximate separator location.

magnetic nulls are found using existing techniques, represented by (red) X's at the endpoints. A hemisphere, represented by a dashed semicircle, is centered around the northern null, labeled 0 (the choice of starting null is arbitrary). At many points on the hemisphere's surface, the magnetic field is traced in both directions to determine its topology (open, closed, or half-open). The point at which all topologies meet is where the separator intersects the hemisphere; we mark this intersection with a (blue) x and label it location 1. A new hemisphere is centered at location 1 and the separator's intersection with this new hemisphere is determined similarly. This new intersection is marked by another (blue) x, labeled as location 2. This process is repeated until the southern null, labeled n + 1, is inside a hemisphere. The separator is mapped by connecting the nulls to the individual separator locations in order (0 through n + 1), sketched as the solid (black) line.

We now provide a more detailed description of the steps in this technique. To locate the magnetic nulls, we use the method described by *Haynes and Parnell* (2007). Since global minima of the magnetic field magnitude $|\mathbf{B}|$ do not faithfully locate magnetic nulls, every grid cell where all three components of the magnetic field change sign is flagged. The field is then linearized within these flagged cells and a Newton-Raphson iteration algorithm is used to locate magnetic nulls at sub-grid resolution.

Having identified the nulls, we proceed to map the separator. Each hemisphere in the iteration has a fixed radius $R_{\rm HS}$ (hemispheres are used to automatically prevent retracing in the opposite direction). Points on the hemisphere's surface are mapped by a set of angular coordinates (ϕ, λ), where ϕ is the longitude measured from the $+x$-axis in GSE coordinates and λ is the latitude. In spherical coordinates, $\lambda = 90^\circ - \theta$, where θ is the polar angle measured from the $+z$-axis in GSE.

The hemisphere's surface is discretized into a $N_\phi \times N_\lambda$ grid and the topology of the magnetic field is determined at each grid point (we use a 36×36 grid). To calculate magnetic topology, we use the Kameleon software package developed at NASA's CCMC. We perform a bi-directional trace of the magnetic field at each point on the surface, using the field's footpoints to determine its topology. A field line is closed if both footpoints are within 5 R_E of the origin and is open if both do not. Half-closed field lines have one footpoint within 5 R_E of the origin. If the footpoint close to the origin has a negative z-coordinate, then the field line is a southern half-closed field line. Conversely, a northern half-closed field line has the connecting footpoint with a positive z-coordinate. Each point on the hemisphere is coded by its topology. An example is in Fig. 4; closed magnetic fields are colored red, open magnetic fields are orange, southern half-closed fields are black, and northern half-closed fields are white.

To identify where the four topologies meet, interpolation is usually necessary. The separator lies in between the northern and southern half-closed regions. We start by searching through the topological map for the locations where these regions are closest. In Fig. 4, the two closest points are at $(0^\circ, -30^\circ)$ and $(-20^\circ, -28^\circ)$. We find the topology of the field line through the midpoint of the line connecting these points. Then, we march out along the line perpendicular to this line until the topology changes. The separator location is defined as the average of the two points with differing topologies. Figure 4 displays a

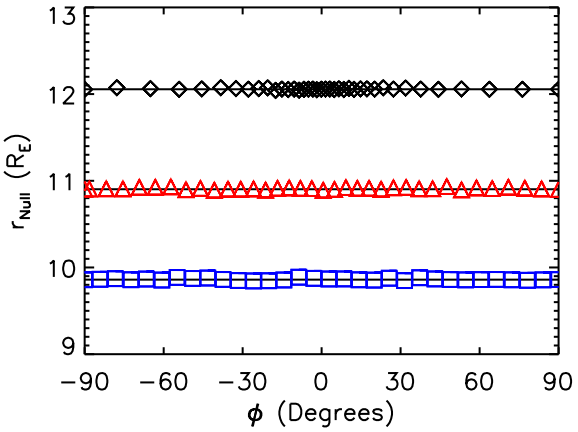

Figure 5: Verification of the separator tracing algorithm for $\theta_{\rm IMF} = 30°$ (black diamonds), 90° (red triangles), and 150° (blue squares) using vacuum superposition. The exact solutions for the separator are shown as solid (black) lines.

(black) asterisk at its approximate separator location which reasonably estimates where the four topologies meet.

The separator location is used as the center of the subsequent hemisphere. If the separator intersects the k-th hemisphere at longitude and latitude (ϕ_k, λ_k), the coordinates of the next hemisphere's center $\mathbf{r}_{k+1}$ are

$$\mathbf{r}_{k+1} = \mathbf{r}_k + \mathbf{r}\left(R_{\rm HS}, \phi_k, \lambda_k\right), \tag{1}$$

where $\mathbf{r}_k$ is the center of the k-th hemisphere, and $\mathbf{r}\left(R_{\rm HS}, \phi_k, \lambda_k\right)$ is the separator's location on the k-th hemisphere in spherical coordinates relative to $\mathbf{r}_k$. A range of $[\phi_k - 90°, \phi_k + 90°]$ is used as the longitude of $k+1$-st hemisphere; this explains why the horizontal axis in Fig. 4 is not centered around $\phi = 0°$. An arbitrary degree of accuracy can be obtained by decreasing the radius $R_{\rm HS}$ and/or increasing the number of grid points N_ϕ, N_λ on the hemispheres.

The method described here has some similarities to the four field junction method by *Laitinen et al.* (2006). This method calculates the magnetic topology at every point on a Cartesian grid near regions where the separator is thought to exist. The separator is approximated by locations where all four topologies are within 3 grid cells of each other, resulting in a ribbon-like structure at the dayside magnetopause. Our method does not require a priori knowledge of the separator's location, as it starts from the nulls and traces the complete separator. It is also computationally inexpensive, since the magnetic topology is calculated on a number of surfaces rather than a volume at the dayside magnetopause.

To test this technique, we use a simple magnetic field model with analytic solutions for the nulls and separators (*Yeh*, 1976; *Hu et al.*, 2009). We superpose a dipolar magnetic field $\mathbf{B}_{\rm D}$ with a uniform background magnetic field $\mathbf{B}_{\rm IMF}$ that makes an angle $\theta_{\rm IMF}$ with the z-axis. The vacuum superposition magnetic field $\mathbf{B}_{\rm VS}$ is given by

$$\mathbf{B}_{\rm VS}\left(\mathbf{r}\right) = \mathbf{B}_{\rm D}\left(\mathbf{r}\right) + \mathbf{B}_{\rm IMF}. \tag{2}$$

We use this technique to trace separators in vacuum superposition with $\theta_{\rm IMF} = 30°$, 90°, and 150°. The separator locations are plotted in Fig. 5 as (black) diamonds for $\theta_{\rm IMF} = 30°$, (red) triangles for 90°, and (blue) squares for 150°. The exact solutions for the vacuum superposition separator are plotted as solid (black) lines. The measured separator locations agree exceedingly well with the exact solutions. See *Komar et al.* (submitted to J. Geophys. Res.) for a more detailed description of the developed technique's verification.

4 Results and Discussion

4.1 The Magnetic Nulls

We find the magnetic nulls in our MHD simulations by employing the *Haynes et al.* (2007) method and their GSE locations are displayed in Fig. 6 as function of IMF clock angle. Figure 6 displays the measured MHD

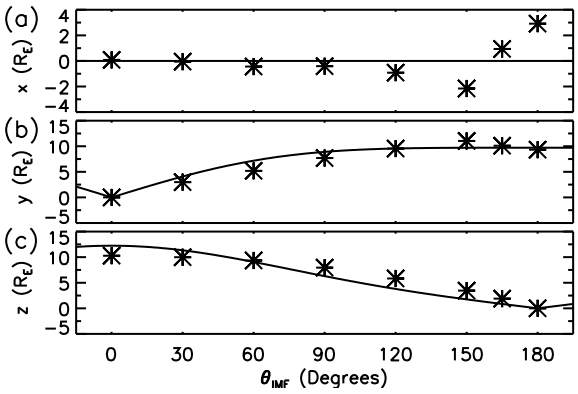

Figure 6: Plots of magnetic null (a) x-coordinate, (b) y-coordinate, and (c) z-coordinate (GSE) as a function of IMF clock angle $\theta_{\rm IMF}$. Solid lines display vacuum superposition solutions and asterisks are the coordinates of nulls in the MHD simulations.

coordinates of the nulls as asterisks and the solid lines as the predicted values in the vacuum superposition field given by Eq. 2. The y- and z-coordinates of the nulls follow qualitatively similar trends for both vacuum superposition and MHD, whereas the x-coordinate in the vacuum superposition fields does not capture the trend found in the MHD simulations [see *Komar et al.* (submitted to J. Geophys. Res.) for a more detailed analysis].

4.2 The Magnetic Separators

The separator tracing method described in Sec. 3 is used to trace the dayside separators for the MHD simulations. We start from the magnetic nulls described in the previous section and use hemispheres with radii of $R_{\rm HS} = 1$ R$_{\rm E}$ to trace the separators. The separators traced for clock angles 30° through 180° are displayed in Fig. 7. Panel (a) displays the separators looking duskward along the y-axis and (b) displays the separators looking Earthward along the x-axis.

Care must be taken in tracing the separator for $\theta_{\rm IMF} = 180°$ due to the infinite number of nulls in the ecliptic plane. We start by centering a sphere at the subsolar point $\mathbf{r}_{\rm Null} = (7.87, 0.00, 0.00)$ R$_{\rm E}$. We center the hemisphere at the subsolar point, and the hemisphere is discretized into the same $N_\phi \times N_\lambda$ grid as described in Section 3. The hemisphere's coordinates span longitude $0° \le \phi \le 180°$ and latitude $-90° \le \lambda \le 90°$. The chosen longitude range only traces the portion of the separator duskward of the subsolar point. The algorithm iteratively marches in the ecliptic plane until it no longer detects a merging location, ending at $\mathbf{r} = (2.93, 9.33, 0.00)$ R$_{\rm E}$. The dawnward portion of the separator is traced likewise by forcing the hemisphere to have a longitude range of $-180° \le \phi \le 0°$, ending at $\mathbf{r} = (2.93, -9.33, 0.00)$ R$_{\rm E}$. The resulting separator is stitched together with the subsolar point as the center of each portion.

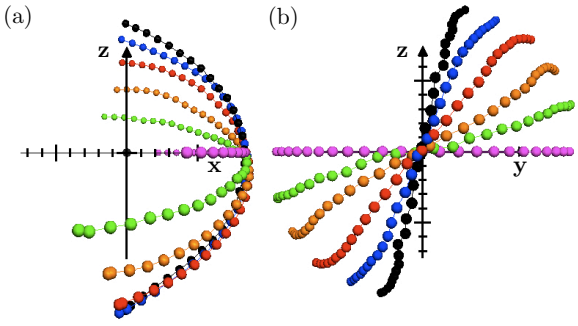

Figure 7: Plot of separators in global MHD simulations for $\theta_{\rm IMF} = 30°$ (black), 60° (blue), 90° (red), 120° (orange), 150° (green), 180° (purple) looking (a) duskward and (b) earthward.

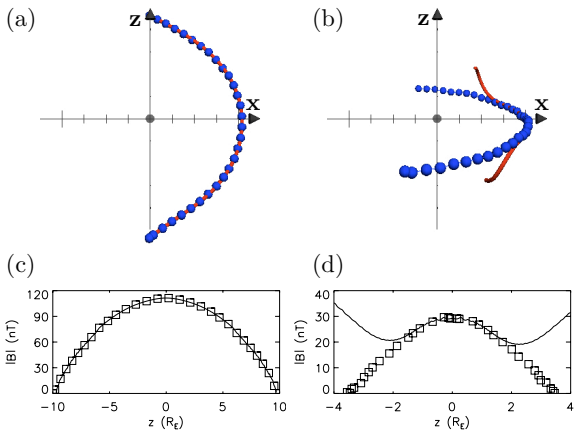

Figure 8: Comparison between traced separators and the last closed field line in global MHD simulations. The last closed field line is a solid (red) line and the determined separator locations are (blue) spheres for $\theta_{\rm IMF}$ of (a) 30° and (b) 150°. The magnetic field strength $|\mathbf{B}|$ as a function of z-coordinate along the separator is a solid line for the last closed field line and as squares for the traced separator for $\theta_{\rm IMF}$ (c) 30° and (d) 150°.

4.2.1 Comparison with the Last Closed Field Line

The last closed field line on the sun-Earth line has been used to approximate the magnetic separator since it closely approaches both magnetic nulls [northward IMF: (*Dorelli et al.*, 2007); southward and northward IMF: *Hu et al.* (2009)]. We compare the traced separators with the last closed field lines on the x-axis for two different clock angles. Figures 8(a) and (b) show the last closed field line as a solid (red) line and the individual locations determined by the method described in Sec. 3 as (blue) spheres for $\theta_{\rm IMF} = 30°$ and 150°, respectively. The traced separator and last closed field line are nearly identical in (a), where the IMF has a northward B_z. In contrast, the two have a large deviation in (b), where the IMF has a southward B_z. Panels (c) and (d) display $|\mathbf{B}|$ as a function of separator z-coordinate along the separator, with the last closed field line shown as a solid (black) line and the locations of the traced separator plotted as squares for the same two cases. The last closed field line and the traced separator are coincident in (c) and, importantly, both connect with the magnetic nulls. In (d), the traced separator closely agrees with the last closed field line near the subsolar point, but only the traced separator connects with the magnetic nulls, while the last closed field line diverges strongly. More generally, we find that both methods agree near the subsolar point for all $\theta_{\rm IMF}$, but as $\theta_{\rm IMF}$ increases from 90°, the last closed field line increasingly deviates from the traced separators. Therefore, the last closed field line does not accurately map the entire separator for southward B_z in our simulations. While the last closed field line is accurate for northward B_z, the method of Sec. 3 works for any clock angle.

4.2.2 Clock Angle Dependence of MHD Separators

We now turn to comparing separators for different clock angles. Each separator is roughly coplanar, and is tilted around the x-axis by an amount dependent on the clock angle. To quantify the structural properties of the separator, we define the separator tilt angle κ at the subsolar point measured with respect to the z-axis. The tilt angles of the separators are measured as the angle relative to $\hat{\mathbf{z}}$ of the last closed field line at the subsolar point. To investigate the separator shape as a function of clock angle, we rotate clockwise around the $+x$-axis by κ and display the separator's projection in this rotated plane. The coordinate system (x', y', z') for this rotated plane has x' pointing sunward, z' in the plane of the separator pointing northward and duskward, and y' completes the triplet.

Figure 9(a) shows the separator's projection in the rotated plane for different IMF clock angles $\theta_{\rm IMF}$: 30° as (black) pluses, 60° as (red) asterisks, 90° as (blue) diamonds, 120° as (green) triangles, 150° as (purple) squares, 165° as (gray) X's, and 180° as (green) pluses. The symbol size denotes the location's deviation from the plane, with smaller symbols indicating a larger deviation from the plane. Figure 9(a) simultaneously

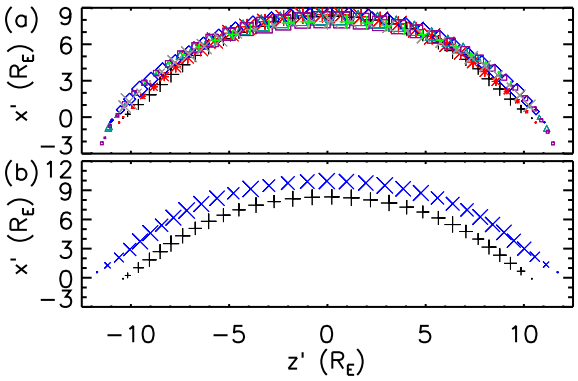

Figure 9: MHD separators rotated around $\hat{\mathbf{x}}$ into a common plane. (a) Separators for the different clock angles are: 30° (black plus), 60° (red asterisk), 90° (blue diamond), 120° (green triangle), 150° (purple squares), 165° (grey X), and 180° (green plus). (b) Plot of MHD separators with $\theta_{\rm IMF} = 30°$ with solar wind number density $n = 20$ cm^{-3} (black plus) and $n = 5$ cm^{-3} (blue X). Symbol size is inversely related to the deviation from the plane.

quantifies three structural features of the magnetic separators. It is clearly seen that the separators maintain a similar shape regardless of $\theta_{\rm IMF}$. Also, the separators rotate around the magnetopause for increasing $\theta_{\rm IMF}$, turning clockwise around the x-axis. Finally, the symbols indicate that a large portion of the separator is approximately coplanar in the plane defined by κ, particularly at the nose of the magnetosphere where the deviation from the plane is ≤ 0.2 R$_{\rm E}$. The deviation is larger near the nulls ($\simeq 1.5$ R$_{\rm E}$), which can clearly be seen in Fig. 7(b), where the ends of the separators flare towards the dawn and dusk flanks. This implies that it is not accurate to model separators as lying in the plane of the nulls.

To gain perspective on the observed trends in separators in MHD simulations with varying IMF clock angle, we compare them to vacuum superposition separators, although a perfect correlation is not expected. As discussed earlier, MHD separators are mostly coplanar; the vacuum superposition separators are exactly coplanar. Also, the shape of the separator is different between the models. In vacuum superposition, the separator is a circular arc. The MHD separators exhibit the well known bullet shape of the magnetopause, as seen in Fig. 9.

The separator tilt angle dependence on IMF clock angle is displayed in Fig. 10. The black pluses display κ for our MHD simulations. The tilt angle solution for vacuum superposition separators is displayed as the dashed (blue) line (*Yeh*, 1976; *Hu et al.*, 2009). Lastly, the solid (red) line shows $\theta_{\rm IMF}/2$, the angle bisecting the IMF and terrestrial magnetic field, a commonly used estimate, for reference.

The MHD separator tilt angle κ increases from 0° to 90° for vacuum superposition, MHD, and angle of bisection. The tilt angles for the three κ values are relatively close to each other, within about 20°. However, quantitative predictions and trends with clock angle reveal important differences between the models. In

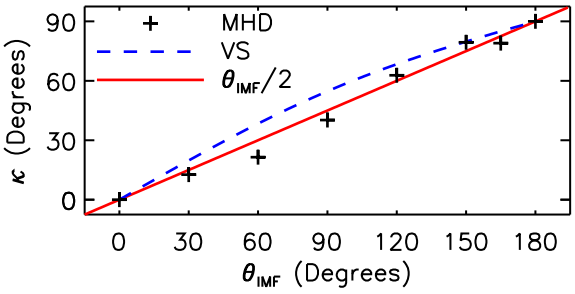

Figure 10: Separator tilt angle κ at the subsolar point as a function of IMF clock angle $\theta_{\rm IMF}$. The solid (red) line is the bisection angle $\theta_{\rm IMF}/2$, the dashed (blue) line is for vacuum superposition separators and the pluses are for MHD separators.

vacuum superposition, the tilt angle is consistently larger than the angle of bisection, implying separators that are tilted towards the ecliptic plane. MHD separators are tilted towards the noon-midnight meridional plane for $\theta_{\rm IMF} \leq 90°$, but are tilted towards the ecliptic for $\theta_{\rm IMF} = 120°$ and $150°$. Therefore, the three models follow similar trends at small and large IMF clock angles, but the MHD separator tilt angle displays significant differences from the models for intermediate clock angles.

4.2.3 Density Dependence of Separators

As a preliminary test of the parametric dependence of MHD separator characteristics, we perform a simulation similar to our $\theta_{\rm IMF} = 30°$ simulation, only changing solar wind number density to $n = 5$ cm^{-3} (from $n = 20$ cm^{-3}). We expect the magnetosphere to expand with this decrease in number density. The location of the magnetopause $R_{\rm MP}$ on the x-axis occurs approximately where the solar wind dynamic pressure balances the magnetosphere's magnetic pressure. As the magnetospheric magnetic field is dipolar with $B_{\rm D} \propto 1/r^3$, the magnetopause location $R_{\rm MP}$ depends on density as $R_{\rm MP} \propto n^{-1/6}$. For these simulations, this implies the magnetopause should expand by a factor of $(5/20)^{-1/6} \simeq 1.26$. The measured values of $R_{\rm MP}$ from the simulations are 9.94 $R_{\rm E}$ for $n = 5$ cm^{-3} and 8.32 $R_{\rm E}$ for $n = 20$ cm^{-3}, giving a ratio of $\simeq 1.20$, in excellent agreement with expectations. The magnetic nulls of the lower density run are sunward and radially outward from their high density counterparts. This behavior is due to the expansion of the magnetosphere with a lower solar wind density. Thus, the magnetic null locations are sensitive to the solar wind density.

The expansion of the magnetosphere also affects separator location. Figure 9(b) displays the separators for the two simulations rotated into the principle plane of the separator. The original high density run is displayed as (black) pluses and the low density run as (blue) X's. As expected, the $n = 5$ cm^{-3} separator expands outward in the x'-z' plane. We measure the separator tilt angle in the lower density simulation and find that the tilt angle is very similar to that of the higher density simulation, suggesting that the separator's tilt angle is not strongly dependent on solar wind number density (for the chosen simulation parameters).

5 Conclusions

In summary, we present an analysis of global magnetospheric BATS-R-US simulations requested through CCMC's Runs-On-Request feature. The simulation data was analyzed and characterized using CCMC's Kameleon, Space Weather Explorer, and on-line visualization tools. The work presented details a new, efficient and highly accurate method to trace magnetic separators in global magnetospheric simulations. The method is to start at a magnetic null and iteratively trace the dayside separator by calculating the magnetic topology on the surface of spherical shells to locate regions of topological merging. We verify the method using a simple magnetic field model with analytic solutions for the separators, and find the method improves on previous ones by being efficient and working for any IMF clock angle. We use the developed method to trace separators in several distinct resistive global MHD magnetospheric simulations with $\theta_{\rm IMF}$ ranging from 0° to 180°. The resulting magnetic nulls and separators in MHD simulations are compared to those in the analytic magnetic field model. As the IMF clock angle increases, the separators maintain a similar shape, and a large portion of the separators are approximately coplanar. A preliminary test of the separator's dependence on solar wind number density n reveals that separator orientation does not change for our chosen solar wind parameters.

This work employed several simplifying assumptions. The largest assumption is the inclusion of an explicit resistivity, which is done to limit the effect of numerical dissipation. We also constructed our simulations to not have flux transfer events (FTEs) (*Russell and Elphic*, 1978), which would change the separators, as reported by *Dorelli and Bhattacharjee* (2008, 2009). We also assume a quasi-steady state with our choice of constant and uniform solar wind parameters. Future work will involve parametric studies of the dependence of the separator location on solar wind parameters, as well as testing Hall physics and FTEs.

References

Angelopoulos, V., J. P. McFadden, D. Larson, C. W. Carlson, S. B. Mende, H. Frey, T. Phan, D. G. Sibeck, K.-H. Glassmeier, U. Auster, E. Donovan, I. R. Mann, I. J. Rae, C. T. Russell, A. Runov, X.-Z. Zhou,

and L. Kepko (2008), Tail reconnection triggering substorm onset, *Science*, *321*, 931.

Cowley, S. W. H. (1973), A qualitative study of the reconnection between the earth's magnetic field and an interplanetary field of arbitrary orientation, *Radio Science*, *8*(11), 903–913.

De Zeeuw, D., T. Gombosi, C. Groth, K. Powell, and Q. Stout (2000), An adaptive MHD method for global space weather simulations, *IEEE Transactions on Plasma Science*, *28*, 1956.

Dorelli, J. C., and A. Bhattacharjee (2008), Defining and identifying three-dimensional magnetic reconnection in resistive magnetohydrodynamic simulations of Earth's magnetosphere, *Phys. Plasmas*, *15*, 056504.

Dorelli, J. C., and A. Bhattacharjee (2009), On the generation and topology of flux transfer events, *J. Geophys. Res.*, *114*, A06213.

Dorelli, J. C., A. Bhattacharjee, and J. Raeder (2007), Separator reconnection at Earth's dayside magnetopause under generic northward interplanetary magnetic field conditions, *J. Geophys. Res.*, *112*, A02202.

Dungey, J. W. (1961), Interplanetary magnetic field and the auroral zones, *Phys. Rev. Lett.*, *6*, 47.

Dungey, J. W. (1963), The structure of the exosphere, or adventures in velocity space, in *Geophysics: The Earth's Environment*, edited by C. De Witt, J. Hieblot, and A. Lebeau, p. 505, Gordon Breach, New York.

Gombosi, T., D. DeZeeuw, C. Groth, and K. Powell (2000), Magnetospheric configuration for Parker-spiral IMF conditions: Results of a 3D AMR MHD simulation, *Advances in Space Research*, *26*, 139.

Haynes, A. L., and C. E. Parnell (2007), A trilinear method for finding null points in a three-dimensional vector space, *Phys. Plasmas*, *14*, 082107.

Haynes, A. L., C. E. Parnell, K. Galsgaard, and E. R. Priest (2007), Magnetohydrodynamic evolution of magnetic skeletons, in *Proceedings of the Royal Society A: Mathematical, Physical and Engineering Science*, vol. 463, p. 1097.

Hu, Y. Q., Z. Peng, C. Wang, and J. R. Kan (2009), Magnetic merging line and reconnection voltage versus IMF clock angle: Results from global MHD simulations, *J. Geophys. Res.*, *114*, A08220.

Komar, C. M., P. A. Cassak, J. C. Dorelli, A. Glocer, and M. M. Kuznetsova (submitted to J. Geophys. Res.), Tracing magnetic separators and their dependence on IMF clock angle in global magnetospheric simulations.

Laitinen, T. V., P. Janhunen, T. I. Pulkkinen, M. Palmroth, and H. E. J. Koskinen (2006), On the characterization of magnetic reconnection in global MHD simulations, *Annales Geophysicae*, *24*, 3059.

Lau, Y.-T., and J. M. Finn (1990), Three-dimensional kinematic reconnection in the presence of field nulls and closed field lines, *Astrophys. J.*, *350*, 672.

Powell, K. G., P. L. Roe, T. J. Linde, T. I. Gombosi, and D. L. D. Zeeuw (1999), A solution-adaptive upwind scheme for ideal magnetohydrodynamics, *J. Comp. Phys.*, *154*, 284.

Russell, C. T., and R. C. Elphic (1978), Initial ISEE magnetometer results: magnetopause observations, *Space Science Reviews*, *22*, 681.

Siscoe, G. L. (1987), The magnetospheric boundary, in *Physics of Space Plasmas*, edited by T. Chang, G. B. Crew, and J. R. Jasperse, pp. 3–78, Scientific, Cambridge, Mass.

Siscoe, G. L., G. M. Erickson, Sonnerup, B. U. Ö., N. C. Maynard, K. D. Siebert, D. R. Weimer, and W. W. White (2001), Global role of $E_{\|}$ in magnetopause reconnection: An explicit demonstration, *J. Geophys. Res.*, *106*, 13015.

Yeh, T. (1976), Day side reconnection between a dipolar geomagnetic field and a uniform interplanetary field, *J. Geophys. Res.*, *81*, 2140.